ISSN 0031-918X, The Physics of Metals and Metallography, 2015, Vol. 116, No. 12, pp. 1259–1269. © Pleiades Publishing, Ltd., 2015.
Original Russian Text © N.B. Pugacheva, N.P. Antenorova, E.I. Senaeva, 2015, published in Fizika Metallov i Metallovedenie, 2015, Vol. 116, No. 12, pp. 1319–1329.

STRENGTH AND PLASTICITY

Study of the Structure and Properties of Laser-Welded Joints of the Al–Mg–Li Alloy

N. B. Pugacheva, N. P. Antenorova, and E. I. Senaeva

Institute of the Engineering Science, Ural Branch, Russian Academy of Sciences, ul. Komsomol'skaya 34, Ekaterinburg, 620049 Russia

e-mail: nat@ imach.uran.ru

Received April 20, 2015; in final form, June 24, 2015

Abstract—The macro- and microstructures, the distribution of chemical elements and of the values of the microhardness over the width of the zones of remelting and heat-affected zone have been studied after the laser welding of sheets of an Al–Mg–Li alloy. It has been shown that the material of the zone of remelting (1.2 mm thick) represents in itself finely dispersed misoriented dendrites, in the primary branches of which particles of the strengthening δ' phase (Al_3Li) with dimensions of no more than 10 nm and in the interdendrite spaces, dispersed particles of the S phase (Al_2MgLi and $FeAl_2$) have been revealed. The hardness of the material of the zone of remelting was 108–123 *HV* 0.05; the hardness of the basic alloy, 150–162 *HV* 0.05. In the heat-affected zones of thickness 2 mm, the primary recrystallization occurred only in a narrow zone directly at the boundary with the weld. The strength of the welded junction was 470–490 MPa, which corresponds to the regulated degree of strength of the aluminum alloys of this class. The relative elongation of the material of the weld proved to be considerably less than that in the alloy matrix because of the microporosity of the weld material. It is shown that the convective stirring of the melt in the welding pool upon the laser welding made it possible to avoid the appearance of macroscopic defects, but on the microlevel there are observed micropores in the form of spheres with dimensions of 5–50 μm. The solidification of the alloy occurred in such a way that the dendrites had time to grow around the gas bubbles prior to their collapse, forming a sufficiently strong carcass. Inside the dendritic carcass, there have been revealed coarse inclusions (to 200 μm) that consist of oxides (Al_2O_3, Fe_2O_3, MgO, SiO_2, CaO), of an iron-based alloy, and of the host aluminum alloy.

Keywords: laser, welding, heat-affected zone, weld, macrostructure, microstructure, intermetallic compound, microhardness, strength, deformation, recrystallization, fracture, fracture surface

DOI: 10.1134/S0031918X1512008X

INTRODUCTION

Due to the combination of low density, high modulus of elasticity, corrosion resistance, and good weldability, the super-light aluminum alloys of the Al–Mg–Li system are applied in the aviation industry, for example, as the material for the fuselage covering of airplanes. In the domestic aircraft industry, the method of riveting is traditionally used to connect the sheet components made of these alloys. Developments that make it possible to use welding to obtain strong structures are of large interest; however, the techniques of welding of aluminum and its alloys have a number of specific features compared with the welding of steels because of substantial differences in the properties of these materials. Aluminum and its alloys have a thermal conductivity that is approximately five times higher than that of steels; therefore, the heat is intensely removed from the site of welding into the components to be welded, which requires an enhanced heat input compared with the welding of steels [1, 2]. This is extremely undesirable, since aluminum has a low melting point; moreover, its strength is reduced sharply upon heating. Thus, the probability of a detail burning through or melting upon welding aluminum is considerably higher than in the case of the welding of steels. Furthermore, aluminum exhibits a significant foundry shrinkage (two times higher than that of steel); therefore, upon the solidification of the metal of the welding pool, significant internal stresses and strains are developed in it, which lead to the formation of hot cracks.

At present, the following three methods are most frequently used from all known methods of the welding of aluminum, i.e., manual, argon-arc, and semiautomatic [2, 3]. The use of laser welding, which is characterized by a number of advantages, is promising; the high power density of radiation ensures the locality of the metal fusion and the formation of a narrow weld of sufficiently large depth with the form coefficient of more than 2.5; the ultrarapid rates of heating and cooling upon laser action decrease the width of the heat-affected zones, as well as reduce the degree of gas saturation of the alloys, especially when inert gases are used to protect the zone of the welding pool and the heat-affected zone [2–4]. Upon welding of steels and titanium alloys, it was possible to obtain welded joints whose strength is higher than that of the materials to be welded [2, 5, 6]. However, even upon laser welding, obtaining strong joints of aluminum alloys is connected

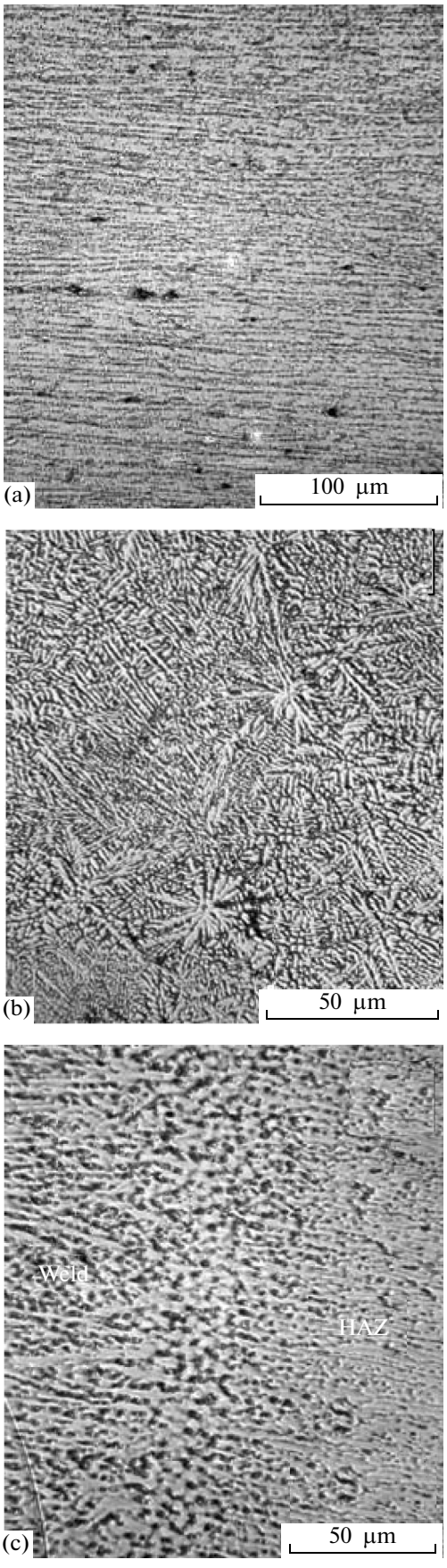

with some specific problems. These primarily include the rapid formation of oxides on the surface, the gas absorption from the environment, and the high reflectivity of aluminum alloys [7, 8]. The structure and properties of the laser-welded joints of the super-light alloys of the Al–Mg–Li system have been quite insufficiently studied to date, and the existing experimental data are contradictory.

The purpose of this work is to study the specific features of the formation, structure, and strength of the welded joints of sheet workpieces of Al–Mg–Li alloy obtained by welding using a CO_2 laser.

EXPERIMENTAL

As the objects of the study, we used sheet workpieces with a thickness of 1.5 mm of an Al–Mg–Li alloy of the following chemical composition (wt %): 6 Mg; 2.2 Li; 0.4 Mn; 0.3 Fe; 0.15 Zr; 0.1 Ti; 0.07 Si; 0.05 Cu; 0.005 Na; Al for balance. The welding was carried out using a CW CO_2 laser and a ZnSe lens with the focal length of 254 mm, under the following conditions: the radiation power $P = 3$ kW; the velocity of the motion of the sample relative to the laser beam, $V = 6.3$ m/min. To protect the surface of the welding pool and of the near-weld zones, a jet of helium was used that was supplied under a pressure of 5.5 atm. The surface of the polished sections prepared from the transverse cut of the weld was investigated by the methods of optical metallography using a NEOPHOT 21 microscope at magnifications of 50–500. The Vickers microhardness was determined using a LEICA VMHT device at a load of 0.5 N. The electron microprobe analysis was performed using a TESCAN VEGAII XMU with an OXFORD attachment. The locality of the analysis was 1 μm with an error of 5% from the measured concentration. The electron-microscopic examinations of thin foils cut out from the weld zone, the heat-affected zone, and the basic alloy were made using a JEM-200CX electron microscope in the regimes of bright field, dark field, and diffraction.

The strength of the joints obtained, namely, the values of the ultimate tearing-off strength σ_u, were estimated based on the results of tests for static tension using an INSTRON 8801 servohydraulic testing machine at a tensile rate of 1 mm/min. The samples for the tests were cut out along and across the rolling direction, and from the regions of the welds in such a way that the welds be in the middle part of the gage part of the samples. The relief of the fracture surface of the samples after mechanical tests was investigated on a TESCAN VEGAII XMU scanning electron microscope and was described using the terms and the basic concepts of fractographic analysis (RD 50-672-88).

Fig. 1. (a) Microstructure of the Al–Mg–Li alloy, (b) the material of the weld, and (c) the heat-affected zone.

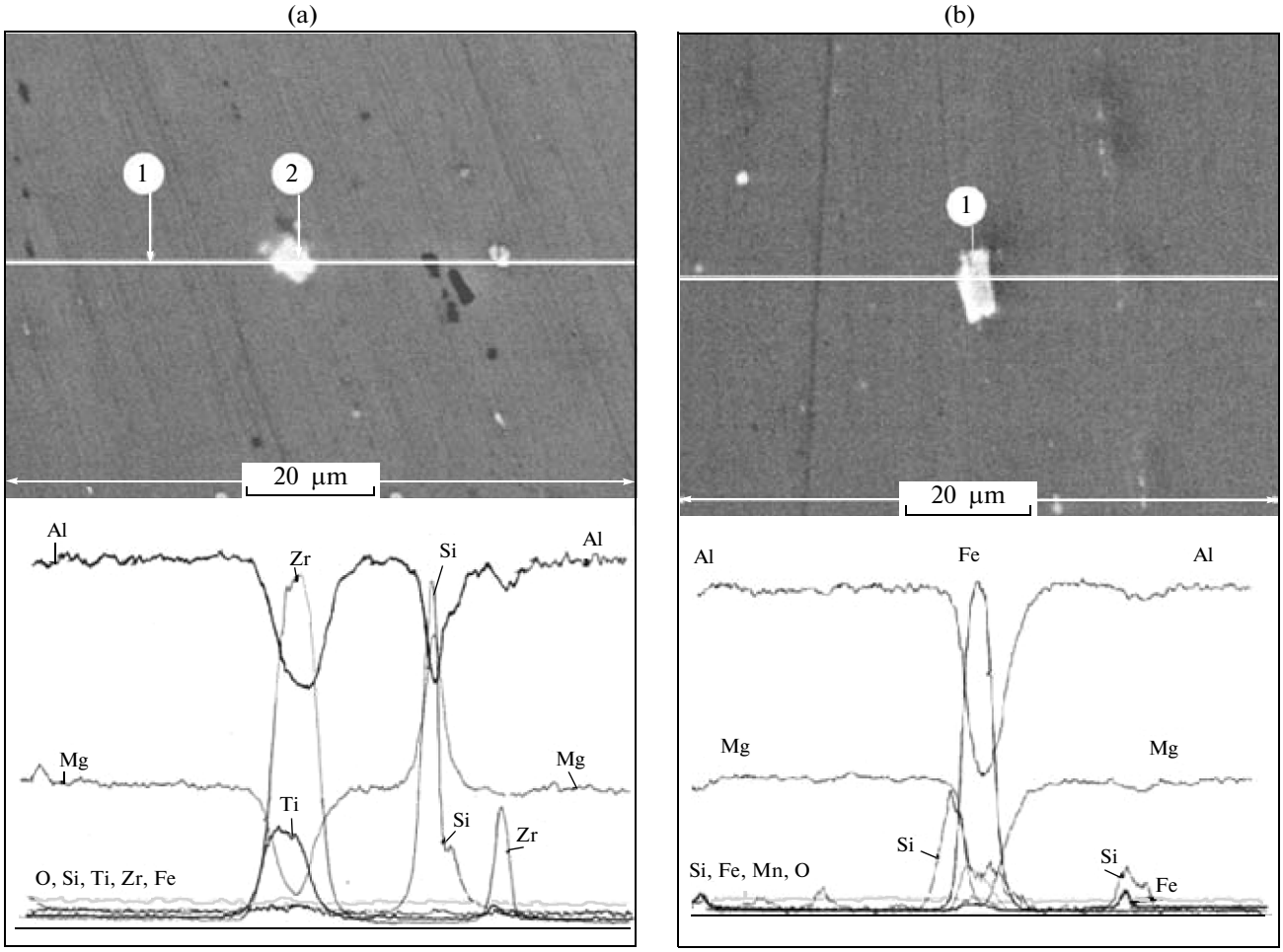

Fig. 2. Distribution of chemical elements in the Al–Mg–Li alloy.

RESULTS AND DISCUSSION

The investigated alloy refers to the heat-treatable wrought aluminum alloys. The basis of the alloy is the α solid solution of the alloying elements (mainly, Li and Mg) in aluminum, the grains in which are elongated along the rolling direction, and the size of which is 40–150 μm in length and 10–20 μm in width (Fig. 1a). Particles of the S1 phase Al_2MgLi are located along the grain boundaries (in the form of almost continuous stitches) and range in size from 0.6 to 3 μm in size. The S1 phase has a cubic structure with 456 atoms in the unit cell and a lattice parameter of 2.03 nm. Magnesium in the alloy forms the Mg_2Si compound with silicon (cubic lattice, structure type $C1$ (CaF_2) with a lattice parameter of 0.6 nm [9]), which is present in the form of separate dark-gray (almost black) particles that are distributed chaotically over the volume of the alloy and have sizes of 100–300 μm (Fig. 2a). Smaller, irregularly shaped inclusions with sizes of 25 × 50 μm contain iron (region 1 in Fig. 2b), which forms the intermetallic compound $FeAl_2$ with an iron content of 31–35 wt %. An increase is always observed in the silicon concentration near these inclusions. Bright inclusions are also present in the alloy, which contain zirconium and, in a smaller amount, titanium (particle 2 in Fig. 2a), in the form of the intermetallic compound $Al_3(Zr,Ti)$. In the bulk of grains, there are observed dispersed particles of the basic strengthening phase δ'-Al_3Li with an ordered $L1_2$ structure that is formed as a result of aging at 120°C of the supersaturated solid solution obtained upon quenching at 450°C. The particles of this phase in the alloy have sizes of 10–30 nm (Fig. 3). As was shown earlier [10–12], the solid solution in this alloy is very stable, and no natural aging occurs in it. The hardness of the basic alloy was 150–162 HV 0.05.

The melting of the aluminum alloy upon the butt welding of sheets occurs at a very high rate under the action of the laser beam. In this case, the welding pool has a form elongated along the direction of the beam motion, as is shown in Fig. 4, a channel (crater) is located in the leading part of the bath and is the region of the brightest glow. The formation of the crater occurs as follows: as soon as the power density of the laser radiation exceeds a certain critical value, the

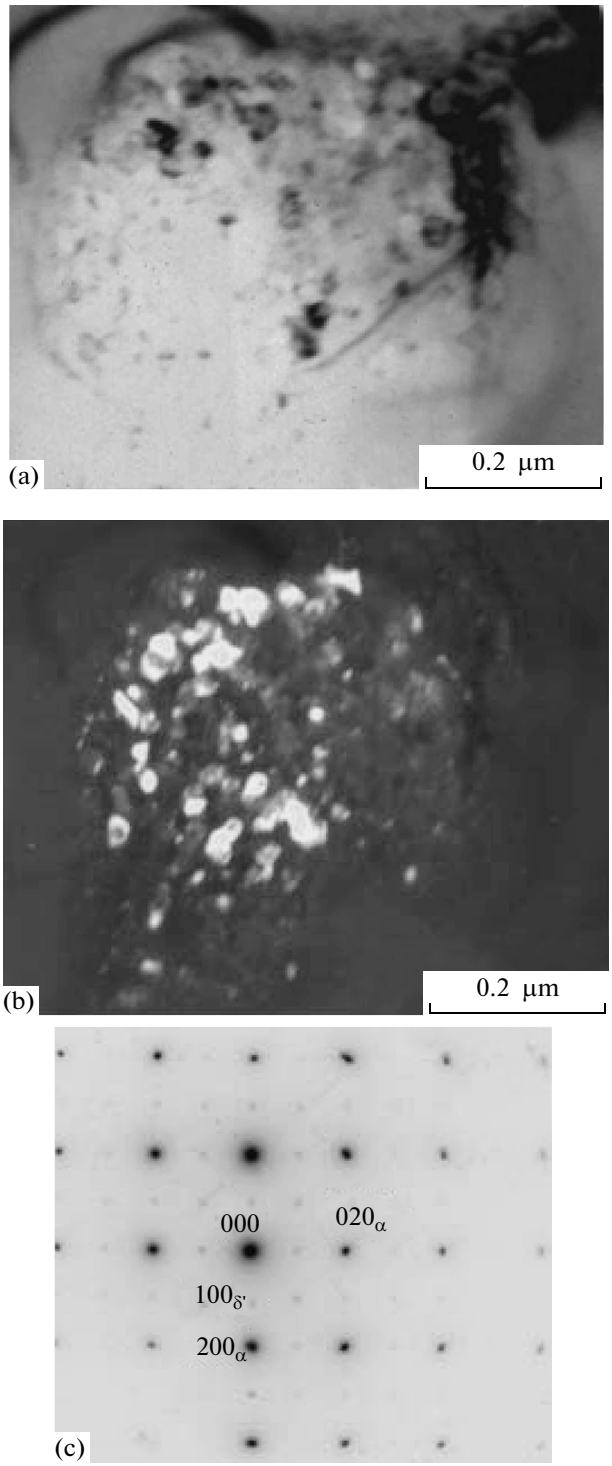

Fig. 3. Electron-microscopic studies of the Al–Mg–Li alloy: (a) bright-field image, (b) dark-field image taken in superlattice reflections $(100)_{\delta'}$; and (c) SAED pattern, zone axis $[001]_{\alpha}$.

heating of the metal occurs at a rate that significantly exceeds the rate of heat removal into the base metal via thermal conductivity [7]. On the surface of the liquid metal, an impression is formed under the action of the

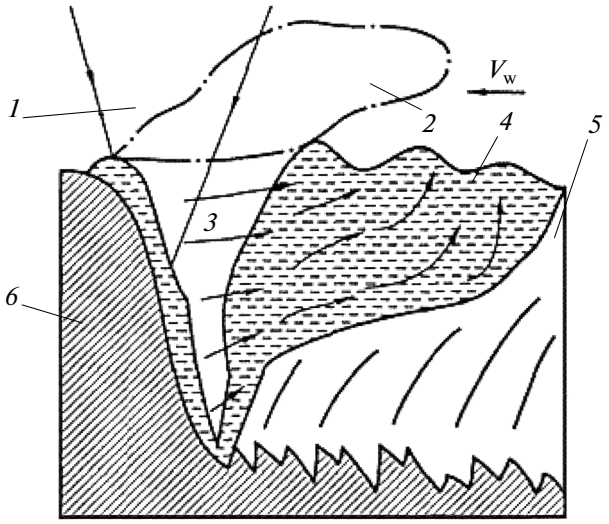

Fig. 4. Scheme of the welding bath upon the laser welding [5]: (*1*) laser beam; (*2*) plasma flame; (*3*) vapor–gas channel; (*4*) tailing part of the bath; (5) crystallized weld metal; (*6*) metal to be welded; V_w, the rate of welding.

boiling of the metal and recoil momentum of the vapors formed. While increasing in size, the impression forms a channel filled with vapors and surrounded by liquid metal. The vapor pressure proves to be sufficient to oppose the forces of hydrostatic pressure and surface tension, and the cavity of the channel is not filled up with liquid metal. With the formation of the channel, there appears a luminous flame above the surface of the metal, which consists of vaporization products, small drops of metal ejected from the bath, and particles of the condensed vapor. Upon the significant rate of welding, the flame deviates by 20°–60° toward the side opposite to the direction of welding. This flame absorbs part of the energy of the laser beam and thereby decreases its melting-through ability [2, 7].

At a certain rate of welding, the shape of the channel became dynamically stable. On the front wall, the metal melts; on the rear wall, the metal solidifies. The presence of the channel favors the absorption of laser radiation in the depth of the material to be welded, rather than only on its surface. This leads to so-called "dagger meltin g-through"; i.e., a narrow weld with a large ratio of the depth of penetration to the width of the weld is formed. The high thermal conductivity of aluminum alloys provides the simultaneous occurrence of two processes: the formation of a channel and surface melting. On the front wall of the channel, there is a layer of molten metal, which experiences continuous perturbations. Here, a characteristic bend of the front wall is observed in the form of a step that periodically moves along the height of the channel. The

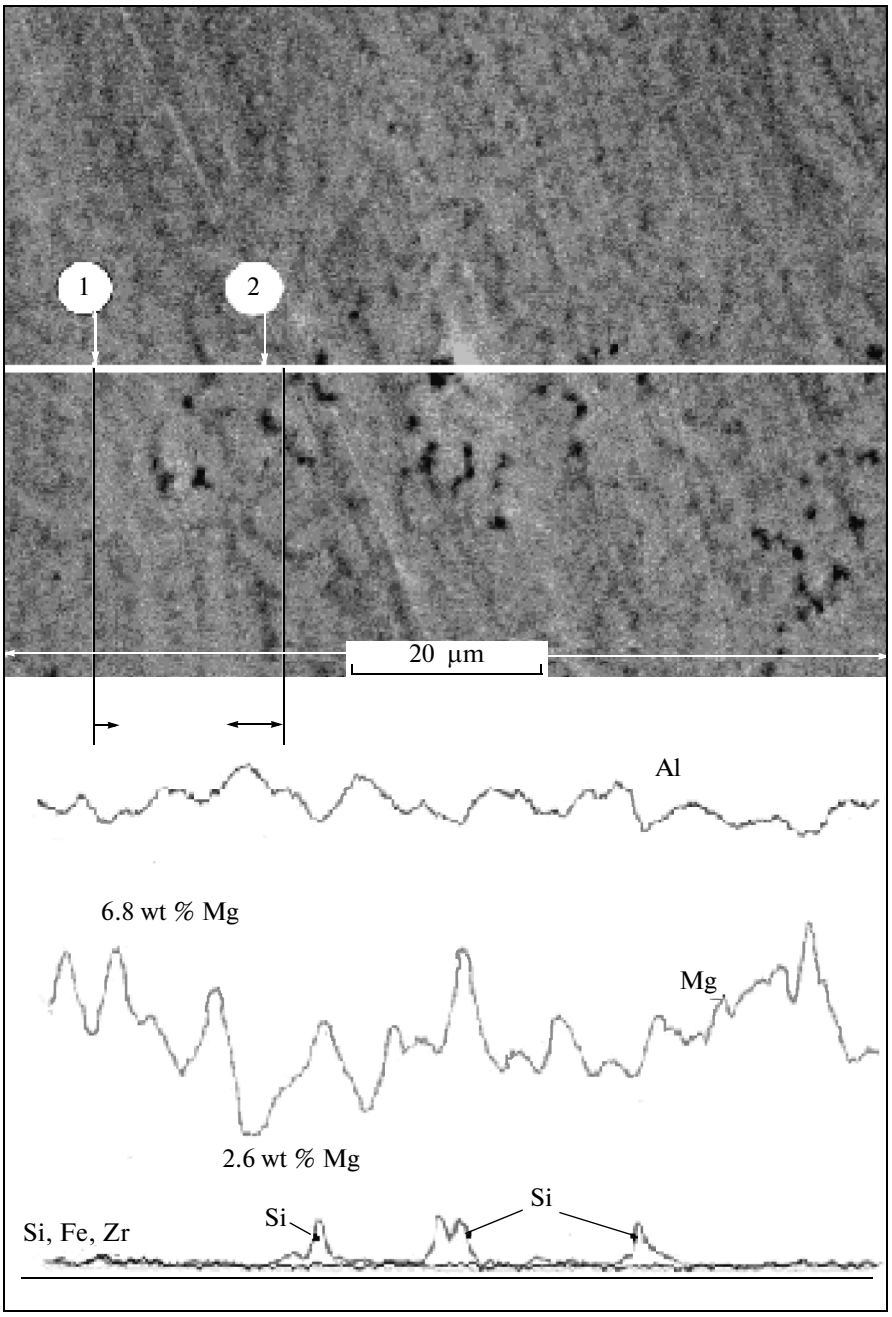

Fig. 5. Distribution of the chemical elements in the material of the weld (central part).

removal of the molten metal from the front wall is accomplished by the displacement of the step from top to bottom. The transfer of the molten metal from the head part of the bath into the tail part occurs along the sidewalls in the horizontal direction. With a deepening of the channel, ascending currents of the melt motion arise [7]. In the tail part of the bath, the molten metal moves upwards by the vortex flows and is carried partially to the surface of the welding pool. The rate of transfer of the melt is three orders of magnitude higher than the rate of welding.

The width of the investigated welds in the cross section was equal to 1.0–1.2 mm; that of the heat-affected zones (HAZ), 2.0 mm. Structurally, the HAZs almost do not differ from the basic alloy (Figs. 1a, 1c). The material of the welds has a misoriented dendritic structure characteristic of the cast alloy in the center of the weld and a columnar dendritic structure near the HAZ (Fig. 1b). The electron microprobe analysis (EMA) showed that the character of the nonuniform distribution of magnesium and aluminum over the width of the welds (Fig. 5) corresponds to the observed

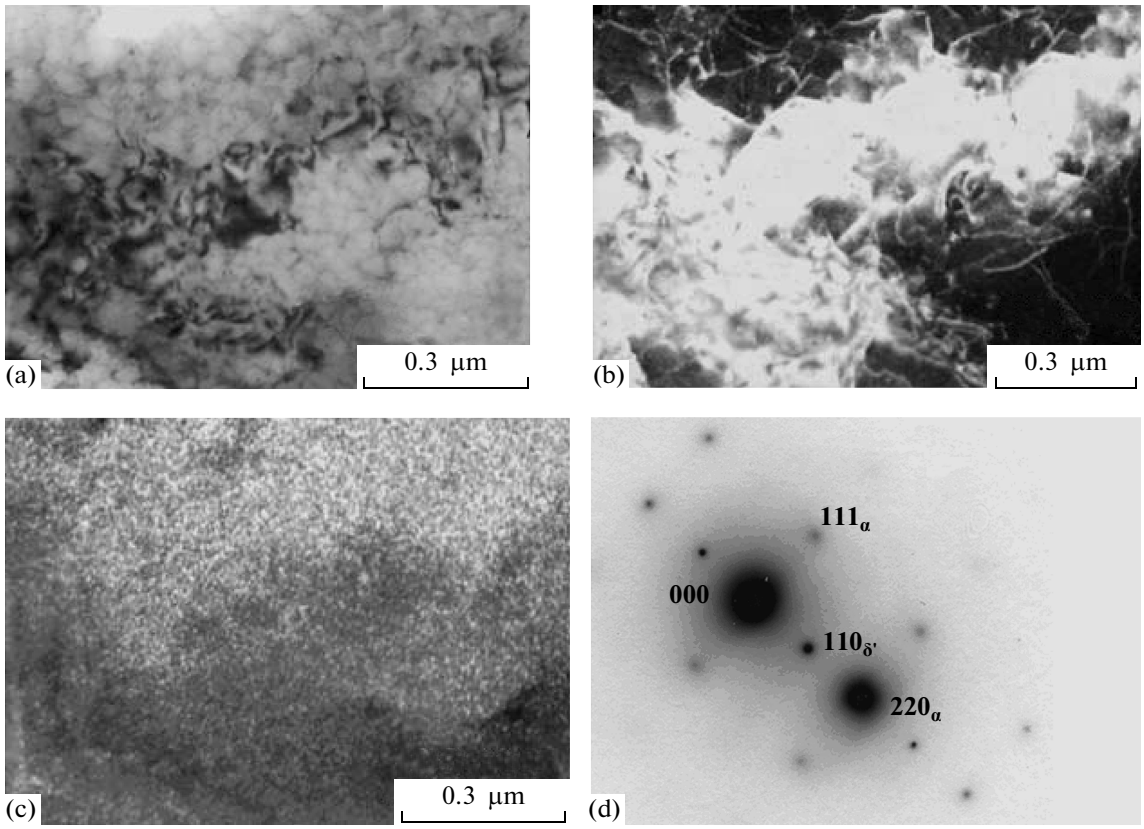

Fig. 6. Electron-microscopic image of the weld metal: (a) bright-field image; (b) dark-field image taken in the superlattice reflection $[220]_\alpha$; (c) dark-field image taken in the superlattice reflection $[110]_{\delta'}$; and (d) SAED pattern, zone axis $[1\bar{1}0]_\alpha$.

dispersed dendritic structure. The dendrite branches are enriched in aluminum; the interdendrite spaces contain an enhanced content of magnesium at the extent of the precipitated dispersed (to 5 μm) particles of the S1 phase Al_2MgLi. In the material of the welds, in spite of the high solidification rates, there is present a finely dispersed strengthening δ' phase Al_3Li; the sizes of its particles are two to three times less than those in the basic alloy and do not exceed 10 nm (Fig. 6). The hardness of the weld material was 108–123 *HV* 0.05; the minimum values of the hardness are observed in the central part (Fig. 7). Almost no particles of $Al_3(Zr, Ti)$ and Mg_2Si were observed in the material of the welds, which can be connected with the very high rate of solidification of the melt, at which the transformations observed in the case of the slow cooling [10–12] have no time to occur.

Values of the ultimate tearing-off strength of the Al–Mg–Li alloy and its welds

Type of samples	σ_u, MPa
Longitudinal samples of the base	525
Transverse samples of the base	558
Welded joint	470–490

In the HAZs, the high rates of heating and cooling upon the laser treatment prevented the occurrence of the processes of recrystallization of the deformed alloy. The narrow zone (of thickness no more than 0.1 mm) of recrystallized grains is only observed at the boundary between the HAZ and the weld (Fig. 1c). The values of hardness in the HAZ decreased compared with the hardness of the basic alloy to 123–138 *HV* 0.05. The minimum values correspond to the recrystallized zone (Fig. 7). Upon the electron-microscopic examinations of the thin foils cut out from the HAZs, small recrystallized grains have been revealed (Fig. 8a); the size of particles of the δ' phase in the HAZs increased in comparison with their size in the basic alloy to 20–40 nm (Figs. 8b, 8c). The particles of Mg_2Si, $FeAl_2$, and $Al_3(Zr, Ti)$ hardly changed in size and shape.

The results of tensile tests showed that the strength of the material of the welds is somewhat lower than the strength of the basic alloy (see table). For these alloys, the value of the ultimate strength must satisfy the condition $\sigma_u \geq 440$ MPa [2]. All the samples tested satisfy

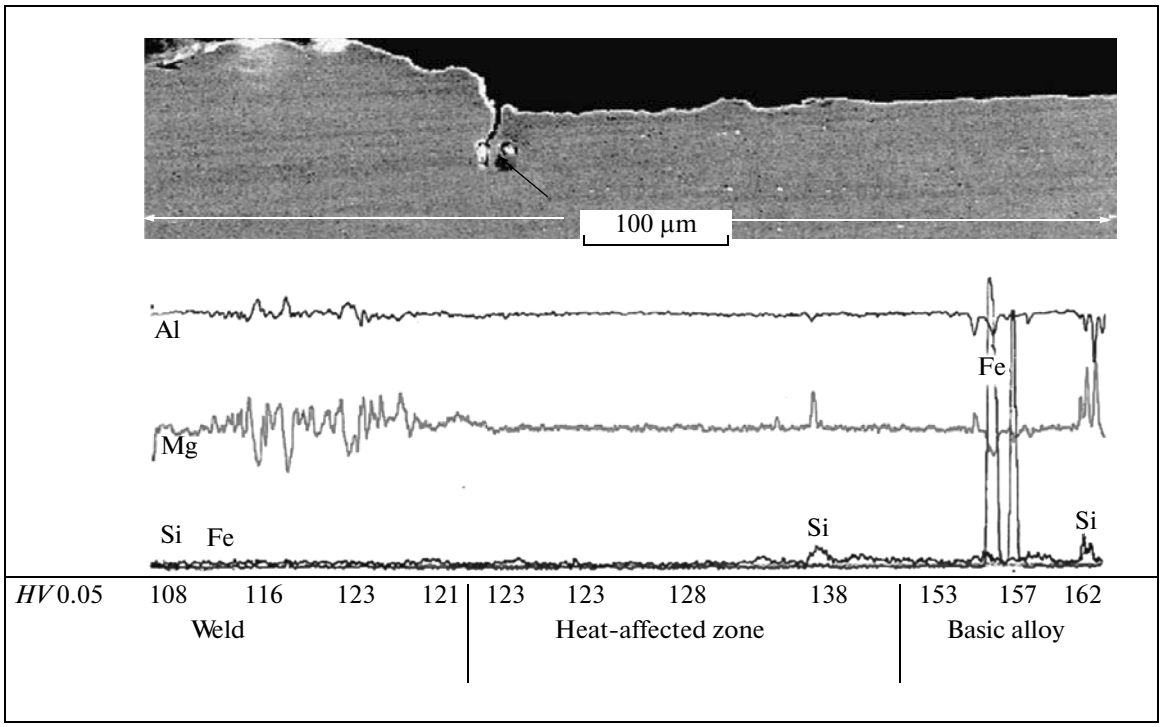

Fig. 7. Distribution of chemical elements and microhardness over the width of the welding joint of the Al–Mg–Li alloy.

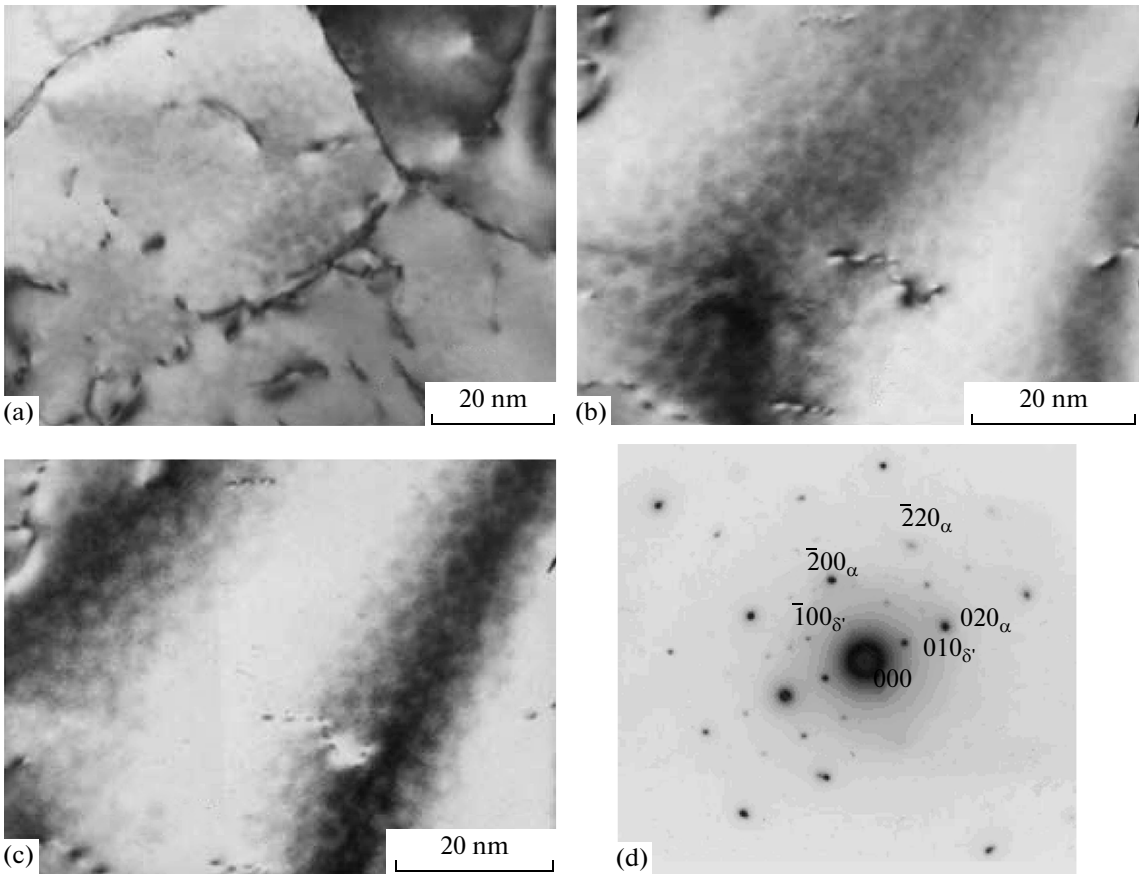

Fig. 8. (a) Grain and the strengthening phase δ'-Al_3Li in the Al–Mg–Li alloy: (a, b) bright-field images; (c) image taken in the superlattice reflection $(010)_{\delta'}$; (d) SAED pattern, zone axis $[001]_\alpha$.

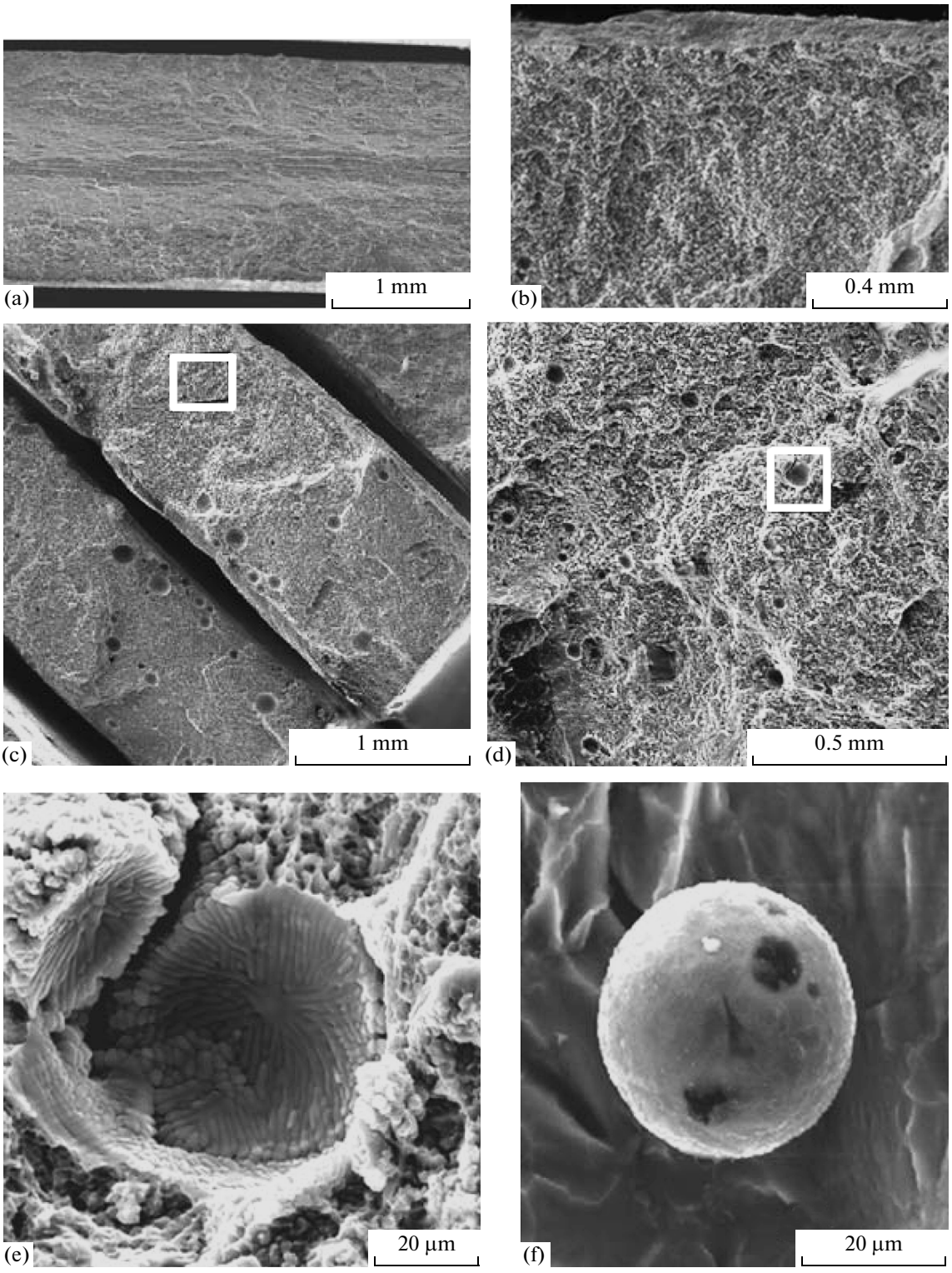

Fig. 9. Relief of the fracture surface of the Al–Mg–Li alloy after static tensile tests (a–e) and bending (f): (a) the sample was cut out across the deformation direction; (b) along the deformation direction; (c–f) material of the weld; (d) region outlined in (c) shown at an enhanced magnification; (e) region outlined in (d) shown at an enhanced magnification.

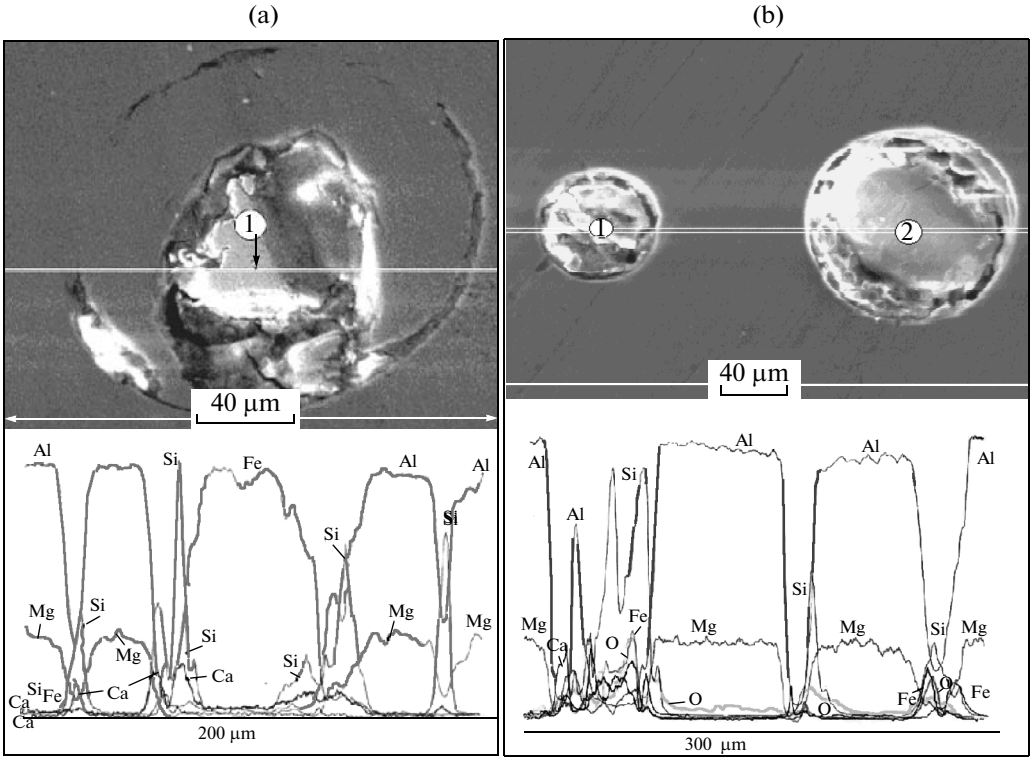

Fig. 10. Distribution of chemical elements over the section of the defects of the weld of the Al–Mg–Li alloy.

this condition, but the relief of the fracture surface of the samples differs substantially. The fibrous-banded relief characteristic of the materials subjected to hot plastic deformation was observed on the fractures of the samples cut out of the sheet of the Al–Mg–Li alloy across the rolling direction, i.e., when the fracture surface was oriented parallel to the direction of the sheet deformation (Fig. 9a). For the sample cut out along the direction of deformation, the fracture surface is oriented in the direction perpendicular to deformation and has a dimpled relief characteristic of the plastic fracture (Fig. 9b).

On the fracture surface of the samples with the weld after tensile tests, spherical pores with a size of 5–200 μm have been revealed (Figs. 9c–9e). Upon the metallographic studies of the cross sections of the welds, no such pores were revealed because of their rubbing by the soft alloy. Therefore, to detect this microporosity, the method of scanning electron microscopy of the fractures of samples after the bending of sheets should be used. In this case, a rupture zone always exists that differs in the surface relief from the major portion of the fracture surface. On the surface of the rupture zone of the investigated samples of the Al–Mg–Li alloy, spherical particles of different sizes of 5–50 μm were revealed (Fig. 9f). An analysis of the chemical composition of the surface of these particles showed that these are particles of aluminum-based Al–Mg–Li alloy. The crystallization of the alloy apparently occurred in such a way that the dendrites had time to grow around gas bubbles before they collapsed and formed a carcass around the micropores, the internal surface of which opens during tensile tests (Fig. 9e). The microporosity affects the behavior of the modulus of elasticity—an important characteristic of the alloys of this class [13].

In the upper part of some welds, single defects are present either in a spherical form or in the form of concentric line, i.e., interlayers located along the boundaries of the spheres (Fig. 10) with sizes of 0.1–0.18 mm. The EMA showed that these concentric interlayers contain silicon in the form of the oxide SiO_2 (Fig. 10a) and that the globular inclusions inside the spheres are inhomogeneous in the chemical composition; they contain oxides (Fe_2O_3, MgO, SiO_2, Al_2O_3, CaO; Fig. 10b, region 1) and an aluminum alloy (Fig. 10b, region 2). In one of the spherical defects, an inclusion of irregular shape represented almost pure iron (Fig. 10a, region 1): 98.2 wt % Fe; 0.09 wt % Si, 0.05 wt % Mn, 0.04 wt % Mg, 0.25 wt % Al). The spherical shape of the inclusions is caused by the minimum surface energy of the particles in the form of spheres in comparison with other forms.

Thus, in the case of the laser welding, the plasticity of the obtained welded joints is limited by the formation of microporosity. At present, there are developments directed toward eliminating the microporosity of the material of welds of aluminum alloys, in particular due to the use of ultrasonic treatment. The authors of [14–16] showed that the ultrasonic treatment of the surface of the welds of aluminum alloys and steels makes it possible to substantially increase their strength and plasticity due to the healing of micropores, as well as due to the refinement of the structure of surface layers.

CONCLUSIONS

The laser welding of 1.5-mm sheets of the Al–Mg–Li alloy investigated makes it possible to obtain welds with a width of 1–1.2 mm, hardness 108–123 *HV* 0.05, and a finely dispersed dendritic structure. In the axes of the dendrites, there are present particles of the strengthening Al_3Li δ' phase with dimensions of no more than 10 nm. No particles of $Al_3(Zr,Ti)$ and Mg_2Si have been revealed in the material of the welds, which can be connected with a very high crystallization rate of the melt upon welding, such the transformations observed in the case of the slow cooling of the alloy have no time to occur.

At the boundary with the weld, heat-affected zones are formed with a thickness of 2 mm, in which the recrystallization has no time to occur. The primary recrystallization with the formation of new equiaxed grains (microhardness 123–128 *HV* 0.05) was only observed directly at the boundary with the zone of remelting, which is of a thickness of no more than 0.1 mm. The strength of the welded joints obtained was 470–490 MPa, which satisfies the requirement that σ_u should be equal to or greater than 440 MPa presented for these alloys.

The fractographic studies of the relief of the fracture surfaces of samples with welds after tension and bending showed that, despite the protection of the weld and the heat-affected zone by a helium atmosphere in the process of laser welding, the melt proved to be saturated by gas. The intensive convective stirring of the melt in the welding pool in the process of laser action made it possible to avoid the appearance of macroscopic defects, but on the microlevel, small micropores are observed with sizes of 5–50 μm. The crystallization of the alloy occurred in such a way that the dendrites had time to grow around the gas bubbles (before the bubbles collapsed) and to form a sufficiently strong carcass. Single pores with sizes to 0.18 mm that are filled with an aluminum alloy Al–Mg–Li, or with Fe_2O_3, MgO, SiO_2, Al_2O_3, and CaO oxides are encountered; the pores also can be filled with virtually pure iron.

The plasticity of the welded joints of the sheets of the Al–Mg–Li alloy obtained using a CO_2 laser is limited by the microporosity of the material of the weld; therefore, subsequently it is of interest to search and develop methods of the elimination of pores both after laser welding (for example, by the ultrasonic treatment of the surface) and by excluding the reasons for their appearance directly during the welding process.

ACKNOWLEDGMENTS

We are grateful to Dr. Vichuzhanin D.I. and to Dr. Kataeva N.V. for the assistance in conducting the studies. The laser welding was carried out at the Khristianovich Institute of Theoretical and Applied Mechanics, Siberian Branch, Russian Academy of Science, under the guidance of Prof. A.M. Orishich. The mechanical tests were performed using the equipment of the Center of Collaborative Access, Institute of the Engineering Science, Ural Branch, Russian Academy of Sciences.

REFERENCES

1. B. A. Kolachev, V. I. Elagin, and V. A. Livanov, *Metal Science and Thermal Treatment of Nonferrous Metals and Alloys* (MISIS, Moscow, 2001) [in Russian].
2. A. M. Orishich, A. N. Cherepanov, V. P. Shapeev, and N. B. Pugacheva, *Nanomodification of Welded Joints at Laser Welding of Metals and Alloys* (Sibir. Otd. Ross. Akad. Nauk, Novosibirsk, 2014) [in Russian].
3. B. Kumar, *Joining of Dissimilar Materials Using Nd:YAG Laser Welding*, Bachelor's thesis. National Institute of Technology, Rourkela, India, (2010).
4. A. Buddery, M. S. Dargusch, D. H. StJohn, J. Drennan, and S. Nabulsi, "Laser welding of titanium and its alloys for medical applications: Current knowledge and future direction," Mater. Sci. Forum **618–619**, 291–294 (2009).
5. N. B. Pugacheva, E. B. Trushina, and N. P. Antenorova, "Effect of laser processing in the microstructure of a structural low-carbon steel," Russ. Metall. (Metally) **2014**, 569–575 (2014).
6. N. B. Pugacheva, D. I. Vichuzhanin, and N. P. Antenorova, "Hardness and character of destruction of welded joints of VT5-1 titanium alloy," Deform. Razrush. Mater., No. 3, 33–38 (2014).
7. A. G. Grigor'yants and I. N. Shiganov, *Laser Technique and Technlogy. In 7 vol. Vol. 5. Laser Welding of Metals* (Vysshaya Shkola, Moscow, 1988) [in Russian].
8. A. M. Zabelin, A. M. Orishich, and A. M. Chirkov, *Laser Technologies in Machine Engineering* (Novosib. Gos. Univ., Novosibirsk, 2004) [in Russian].
9. *Handbook of Refractory Compounds: Properties, Production, Application*, Ed. by T. Ya. Kosolapova (Metallurgiya, Moscow, 1986; Hemisphere Pub. Corp., New York, 1990).
10. G. L. Shneider, "Phase transformations in heat treatment of Al–Li alloys and optimization of operational

properties of semifinished products from these alloys," Metal Sci. Heat Treat. **40**, 27–33 (1998).

11. G. L. Shneider, L. M. Sheveleva, and E. Ya. Kaputkin, "Phase transformations upon heat treatment of 1420 alloy," Tsvetn. Metall., No. 2, 49–52 (1994).
12. I. N. Fridlyander, "Aluminum alloys with lithium and magnesium," Metal Sci. Heat Treat. **45**, 344–347 (2003).
13. S. V. Smirnov, N. B. Pugacheva, M. V. Myasnikova, and E. O. Smirnova, "Heterogeneity of an Al alloy weld and simulation of its elastic deformation," Fiz. Mezomekh. **17**, 51–56 (2014).
14. V. E. Panin, E. N. Kablov, Yu. I. Pochivalov, and V. V. Kolobnev, "Effect of surface nanostructuring on deformation mechanisms and fatigue life of Al–Li alloy 1424. Enhancement of plasticity and technological characteristics," Fiz. Mezomekh. **15**, 107–111 (2012).
15. V. E. Panin, E. N. Kablov, V. S. Pleshanov, V. A. Klimenov, Yu. F. Ivanov, Yu. I. Pochivalov, V. V. Kibitkin, A. A. Napryushkin, O. N. Nekhoroshkov, V. I. Lukin, and S. V. Sapozhnikov, "Effect of ultrasonic shock treatment on the structure and fatigue strength of welded joints of high-strength steel VKS-12," Fiz. Mezomekh. **9**, 85–96 (2006).
16. O. Nekhoroshov, V. Klimenov, H. Kaminskiy, and B. Semukhin, "Ultrasonic impact treatment as a way of increase of welded connections strength," in *Proc. 8th Korea–Russia Int. Symp. on Science and Technology, Tomsk, Russia, 2004*, Vol. 3, pp. 125–127.

Translated by S. Gorin